East European Journal of Physics. **2.** 528-540 (2026)
DOI:10.26565/2312-4334-2026-2-60 ISSN 2312-4334

FORMATION OF AN AXIALLY SYMMETRIC FIELD DISTRIBUTION USING RECTANGULAR APERTURE RADIATORS

I.K. Kuzmychov[1]*, O.A. Voitovych[1], O.S. Lukash[1], E.M. Khutoryan[1], V.P. Maltsev[1], O.V. May[2]

[1]O.Ya. Usikov Institute for Radiophysics and Electronics of National Academy of Sciences of Ukraine, 12, Ac. Proskura str., Kharkiv, 61085, Ukraine
[2]"Actox Ukraine" LLC, 1, Ivana Honty Str., Kyiv, 04112, Ukraine
**Corresponding Author e-mail: kuzmichev.igr@gmail.com*
Received February 24, 2026; revised May 2, 2026; accepted May 22, 2026

Using the aperture method, radiation from the open end of a rectangular waveguide was studied. Expressions were derived to describe the radiation pattern of such an aperture in the far-field region in two mutually perpendicular planes. Numerical studies of the radiation pattern cross-sections in the image plane were performed for two rectangular apertures, 40×33 mm and 30×21.6 mm, with varying aperture widths and heights. A comparison of the obtained radiation pattern cross-sections with a Gaussian field distribution showed that up to the –11 dB level, the radiation pattern cross-sections in both image planes practically coincide with the Gaussian field distribution. This result is particularly important when a wave beam is incident on the flat face of an axicon. It was also shown that varying the smaller dimension of the rectangular aperture can yield an axially symmetric radiation pattern. Experimental studies of these apertures in the K_a band were conducted. Good agreement between the experimental results and theoretical calculations was demonstrated. It was found that when the geometric dimensions of the rectangular aperture exceed two wavelengths, a traveling-wave regime is established in the waveguide section. Experimentally, it was found that the amplitude distribution of the field for both apertures in the far-field region coincides with the Gaussian distribution down to –8.7 dB. It was shown that the use of rectangular apertures to illuminate the flat face of an axicon with a wave beam is impractical.
Keywords: *Aperture method; K_a-band; Rectangular aperture; Radiation pattern; Gaussian field distribution; Axicon*
PACS: 41.20.Cq, 07.57.Hm

1. INTRODUCTION

When exposed to high-power pulsed electromagnetic radiation, voltages on semiconductor components can reach hundreds of volts, potentially causing a malfunction. If the affected equipment contains such components — for example, communications hardware or the input circuits of unmanned aerial vehicles (UAVs) — pulsed irradiation can drive devices into saturation or cause outright failure, effectively disabling them. Compact pulsed sources with high peak power are available in the X-band [1-3], but producing comparable devices in the K_a-band presents challenges. These difficulties stem from increased ohmic losses in electrodynamic elements as frequency rises and from reduced efficiency of energy exchange between the electron beam and the high-frequency field in resonant structures [4]. Consequently, the output pulse power typically decreases in the K_a-band.

Therefore, investigating the effects of high-power pulsed electromagnetic radiation on UAV input circuitry is an important and timely research topic. Several high-power pulse systems have been reported in the literature and open sources. One example is the THOR (Tactical High-Power Microwave Operational Responder) system developed at the U.S. Air Force Research Laboratory. THOR employs ultra-wideband pulses to disrupt UAV operation and reportedly can protect airspace out to approximately 5 km, with peak pulse powers on the order of 150 kW.

The PHASER system, developed by Raytheon, is another well-known, powerful microwave source mounted on top of a six-meter shipping container-like box coupled with radar (e.g., the MPQ-64 Sentinel or Close Combat Tactical Radar) to detect and localize UAVs and to direct pulses toward them. Publicly available information on PHASER's radiator parameters, pulse duration, and output power is limited; its antenna is described as a rectangular panel used with a steerable reflective mirror. The Tesla transformer is apparently used in both systems to generate powerful ultra-wideband pulses.

Epirus Technologies' Leonidas anti-drone system is an example of a compact, high-power X-band microwave solution. Leonidas is lightweight and vehicle-mountable, facilitating rapid deployment. The system has been procured by the U.S. Army; compared with earlier Epirus designs, its effective range against UAVs is reported to have doubled to about 2 km and its output power to have increased by roughly 30% (contract signed on 17 July 2025).

Given these constraints, operation in the K_a-band is attractive. K_a-band waves can penetrate small openings and shielding in UAV enclosures, potentially damaging both input circuits and shielded microelectronics. The principal obstacle is the lack of compact, high-power K_a-band sources. An alternative to increasing source pulse power is to employ low-divergence beams. Bessel beams are a promising candidate: their weakly diverging spatial profiles can concentrate field strength at a target location more efficiently, allowing lower source power to achieve the electric-field intensities needed to affect UAV electronics.

Cite as: I.K. Kuzmychov, O.A. Voitovych, O.S. Lukash, E.M. Khutoryan, V.P. Maltsev, O.V. May, East Eur. J. Phys. 2, 528 (2026), https://doi.org/10.26565/2312-4334-2026-2-60

The propagation of such beams in open resonators has been studied in the K_a-band [5-7]. Several works have also reported the spatial formation of Bessel beams [8,9]. In particular, the authors of [9] demonstrated a Bessel beam with a diameter of 5.5 mm at a distance of 100 mm in the W-band using a diagonal horn, a convex lens, and an optical element (axicon). In all such implementations, an optical element is required to convert a Gaussian beam into a Bessel beam [10, 11]. It has also been shown [12] that circular waveguides can be effectively used for exciting Bessel beams with the aid of optical elements. This requires that the waveguide's operating mode exhibit an axially symmetric electric-field distribution in the plane of the optical element. In the K_a-band, the most commonly used transmission lines are rectangular waveguides, such as the EIA standard WR-28 (7.11 × 3.56 mm^2) and 7.2 × 3.4 mm^2 waveguides. In these waveguides, the dominant TE_{10} mode supports a linearly polarized electric field. As demonstrated in [13-15], the laser output radiation, which is a circular Gaussian beam, is incident on the flat face of an optical element to efficiently form a Bessel beam at its output. Consequently, in the K_a-band, the optical element must likewise be illuminated by an axially symmetric field in order to generate a Bessel beam. Unlike the optical regime, however, a waveguide radiator is required in the K_a-band to produce such an electric-field distribution.

Two key questions arise in this context: whether it is practically feasible to generate an axially symmetric field using a waveguide radiator, and what the diameter of the corresponding Gaussian-like beam will be in the far field (Fraunhofer zone). Therefore, the objective of this paper is to analyze aperture geometries capable of producing axially symmetric field distributions in the far field that closely approximate a Gaussian profile while maintaining a relatively small diameter at the 1/*e* intensity level.

2. RECTANGULAR APERTURE WITH THE TE_{10} MODE

Radiation from the open end of a rectangular waveguide remains of considerable practical interest [16]. However, the problem of forming a far-field radiation pattern (RP) of a rectangular aperture that closely approximates a Gaussian field distribution has not been fully resolved.

Let us therefore consider radiation from the open end of a rectangular waveguide. The origin of the Cartesian coordinate system is placed in the plane of the waveguide aperture (Fig. 1). The *z*-axis coincides with both the waveguide axis and the direction of propagation of the TE_{10} mode. Since an electric field exists in the aperture (at $z = 0$), a corresponding field is also present in the external region. For this configuration, the aperture field method is most commonly applied. Its use is based on the following assumptions [17]:

- the waveguide opening serves as the radiating aperture;
- the exciting field is zero outside the waveguide aperture ($z > 0$);
- the electric field in the aperture plane ($z = 0$) is identical to that in a waveguide cross-section located several wavelengths away from the opening;
- the waveguide operates in a single mode, namely TE_{10}.

It should be noted that for a specific mode (TE_{10}), the accuracy of the results increases as the aperture size becomes large compared with the wavelength λ.

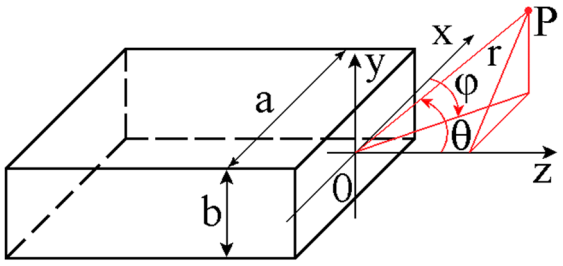

Figure 1. Coordinate systems for studying the radiation of TE_{10} mode from the open end of a waveguide

In the Cartesian coordinate system, the electric-field strength at a point *P* (Fig. 1) can be expressed as follows

$$\vec{E}(P) = E_x(P)\vec{i} + E_y(P)\vec{j} + E_z(P)\vec{k} \tag{1}$$

By analogy with (1), the electric field strength at point *P* in the spherical coordinate system is expressed as follows

$$\vec{E}(P) = E_\theta(P)\vec{e}_\theta + E_\varphi(P)\vec{e}_\varphi + E_r(P)\vec{e}_r \tag{2}$$

The angles θ and φ for the spherical coordinate system are shown in Fig. 1. Let us express the Cartesian coordinates of point *P* through spherical ones

$$\begin{cases} E_x(P) = E_r(P)\sin\theta\cos\varphi - E_\varphi(P)\sin\varphi + E_\theta(P)\cos\varphi\cos\theta, \\ E_y(P) = E_r(P)\sin\varphi\sin\theta + E_\varphi(P)\cos\varphi + E_\theta(P)\sin\varphi\cos\theta, \\ E_z(P) = E_r(P)\cos\theta - E_\theta(P)\sin\theta. \end{cases} \tag{3}$$

A rectangular waveguide supporting the dominant TE_{10} mode ($m = 1$, $n = 0$) is considered. In this case, the electric field has only one nonzero component E_y, while the remaining components $E_x=E_z=H_y=0$. Therefore, in the spherical coordinate system (see Fig. 1), the radial component can be set to zero, $E_r=0$. Taking this into account, expression (3) for the electric-field components of the mode at point P can be written as follows:

$$\begin{cases} E_x(P) = -E_\varphi(P)\sin\varphi + E_\theta(P)\cos\varphi\cos\theta, \\ E_y(P) = E_\varphi(P)\cos\varphi + E_\theta(P)\sin\varphi\cos\theta, \\ E_z(P) = -E_\theta(P)\sin\theta. \end{cases} \tag{4}$$

After substituting the expressions for the electric-field components from equation (4) into equation (1), we obtain a relation in the Cartesian coordinate system that defines the electric-field strength of the TE_{10} mode at point P in terms of spherical coordinates.

$$\vec{E}(P) = \left(E_\theta(P)\cos\varphi\cos\theta - E_\varphi(P)\sin\varphi\right)\vec{i} + \left(E_\varphi(P)\cos\varphi + E_\theta(P)\sin\varphi\cos\theta\right)\vec{j} - E_\theta(P)\sin\theta\vec{k} \tag{5}$$

Taking into account the simplification made ($E_r=0$), the components of the electric field E_θ and E_φ at point P, determined by the electric-field distribution of the TE_{10} mode in a rectangular aperture of cross-section $a \times b$, can be written in the following form in the spherical coordinate system [17]:

$$E_\theta(P) = AZ_0\frac{a^2 b}{\lambda_0^2}\sin\varphi\left(1+\frac{\lambda_0}{\lambda_g}\cos\theta\right)\frac{\cos\alpha}{\alpha^2-(\pi/2)^2}\cdot\frac{\sin\beta}{\beta}, \tag{6}$$

$$E_\varphi(P) = AZ_0\frac{a^2 b}{\lambda_0^2}\cos\varphi\left(\cos\theta+\frac{\lambda_0}{\lambda_g}\right)\frac{\cos\alpha}{\alpha^2-(\pi/2)^2}\cdot\frac{\sin\beta}{\beta}. \tag{7}$$

Here A is the amplitude coefficient, $Z_0=120\pi$ is the wave impedance of free space, $\alpha=(\pi a/\lambda_0)\sin\theta\cos\varphi$, $\beta=(\pi b/\lambda_0)\sin\theta\sin\varphi$, λ_0 is the wavelength in free space, $\lambda_g=\lambda_0\Big/\sqrt{1-(\lambda_0/2a)^2}$ is the waveguide wavelength.

Let us now consider the electric-field component $E_x(P)$ that appears in equations (1) and (5). Substituting into (5) the expressions for $E_\theta(P)$ and $E_\varphi(P)$ given by equations (6) and (7), and omitting the intermediate steps, we can write the result in the following final form:

$$E_x(P) = E_\theta(P)\cos\varphi\cos\theta - E_\varphi(P)\sin\varphi = -D\frac{\lambda_0}{\lambda_g}\sin\varphi\cos\varphi\sin^2\theta, \tag{8}$$

where

$$D = AZ_0\frac{a^2 b}{\lambda_0^2}\frac{\cos\alpha}{\alpha^2-(\pi/2)^2}\cdot\frac{\sin\beta}{\beta}. \tag{9}$$

The expressions for the components of the electric field E_y and E_z, which appear in (1), (5), have the following form

$$E_y(P) = E_\varphi(P)\cos\varphi + E_\theta(P)\sin\varphi\cos\theta = D\left[\cos^2\varphi\left(\cos\theta+\frac{\lambda_0}{\lambda_g}\right)+\sin^2\varphi\cos\theta\left(1+\frac{\lambda_0}{\lambda_g}\cos\theta\right)\right], \tag{10}$$

$$E_z(P) = -E_\theta(P)\sin\theta = -D\sin\varphi\sin\theta\left(1+\frac{\lambda_0}{\lambda_g}\cos\theta\right). \tag{11}$$

By substituting the obtained expressions for the electric-field components $E_x(P)$, $E_y(P)$ and $E_z(P)$, as defined by equations (8), (10), and (11), into equation (5), we obtain the expression for the electric-field strength at point P in the Cartesian coordinate system, expressed in terms of spherical coordinates, as follows:

$$\vec{E}(P) = \left(-D\frac{\lambda_0}{\lambda_g}\sin\varphi\cos\varphi\sin^2\theta\right)\vec{i} + D\left[\cos^2\varphi\left(\cos\theta+\frac{\lambda_0}{\lambda_g}\right)+\sin^2\varphi\cos\theta\left(1+\frac{\lambda_0}{\lambda_g}\cos\theta\right)\right]\vec{j} - D\sin\varphi\sin\theta\left(1+\frac{\lambda_0}{\lambda_g}\cos\theta\right)\vec{k}. \tag{12}$$

By setting $\varphi = 0$ in equation (12), we obtain an expression that describes the RP of a rectangular aperture of cross-section $a \times b$ excited by the TE$_{10}$ mode in the plane of the magnetic-field vector $\vec{H}$ **(**Fig. 1). Taking this into account, equation (12) can be rewritten in the following form:

$$\vec{E}(H) = D\left(\cos\theta + \frac{\lambda_0}{\lambda_g}\right)\vec{j}\,. \tag{13}$$

Let us now consider equation (9). taking into account the notations introduced above:

$$D = AZ_0\frac{a^2 b}{\lambda_0^2}\cdot\frac{\cos\left[(\pi a/\lambda_0)\sin\theta\cos\varphi\right]}{\left[(\pi a/\lambda_0)\sin\theta\cos\varphi\right]^2 - (\pi/2)^2}\cdot\frac{\sin\left[(\pi b/\lambda_0)\sin\theta\sin\varphi\right]}{\left[(\pi b/\lambda_0)\sin\theta\sin\varphi\right]}$$

Since both the ratio $\sin\left[(\pi b/\lambda_0)\sin\theta\sin\varphi\right]/\left[(\pi b/\lambda_0)\sin\theta\sin\varphi\right]$ and $\cos\varphi = 1$ tend to unity at $\varphi \to 0$, we write (9) in its final form

$$D = AZ_0\frac{a^2 b}{\lambda_0^2}\cdot\frac{\cos\left[(\pi a/\lambda_0)\sin\theta\right]}{\left[(\pi a/\lambda_0)\sin\theta\right]^2 - (\pi/2)^2}\,. \tag{14}$$

By substituting equation (14) into equation (13), we obtain:

$$\vec{E}(H) = AZ_0\frac{a^2 b}{\lambda_0^2}\frac{\cos\left[(\pi a/\lambda_0)\sin\theta\right]}{\left[(\pi a/\lambda_0)\sin\theta\right]^2 - (\pi/2)^2}\left(\cos\theta + \frac{\lambda_0}{\lambda_g}\right)\vec{j}\,. \tag{15}$$

An important practical conclusion can be drawn from the analysis of equation (15). The angular dependence of the electric-field strength in the plane of the magnetic-field vector $\vec{H}$ of the TE$_{10}$ mode in a rectangular waveguide of cross-section $a \times b$ is given by the following relation:

$$\cos\left[(\pi a/\lambda_0)\sin\theta\right]/\left[(\pi a/\lambda_0)\sin\theta\right]^2 - (\pi/2)^2\,.$$

This relation is valid for in-phase excitation of a rectangular aperture and for an amplitude distribution of the field within it following the law $\cos(\pi x/a)$. The TE$_{10}$ mode exhibits exactly this distribution of the electric-field strength in the aperture, in the plane of the magnetic-field vector $\vec{H}$.

Upon transitioning to scalar quantities and substituting the meridional angle θ=0 into equation (15), the following expression is obtained:

$$E^{\max}(H) = AZ_0\frac{a^2 b}{\lambda_0^2}\cdot\frac{1}{-(\pi/2)^2}\left(1 + \frac{\lambda_0}{\lambda_g}\right). \tag{16}$$

Using equations (15) and (16), we can write an expression that defines the normalized RP of a rectangular aperture of cross-section $a \times b$, excited by the TE$_{10}$ mode, in the plane of the magnetic-field vector $\vec{H}$ (Fig. 1, $x0z$ plane):

$$\frac{E(H)}{E^{\max}(H)} = 20\lg\left[\frac{\cos\left[(\pi a/\lambda_0)\sin\theta\right]}{\left[(\pi a/\lambda_0)\sin\theta\right]^2 - (\pi/2)^2}\left(\cos\theta + \frac{\lambda_0}{\lambda_w}\right)\times\frac{\left(-\pi^2/4\right)}{\left[1 + \left(\lambda_0/\lambda_g\right)\right]}\right]. \tag{17}$$

Let us now set the azimuthal angle $\varphi = \pi/2$ and analyze the RP produced by a rectangular aperture excited by the TE$_{10}$ mode, in the plane of the electric-field vector $\vec{E}$ (Fig. 1, $y0z$ plane). In this case, equation (12) can be rewritten in the following form:

$$\vec{E}(E) = D\cos\theta\left(1 + \frac{\lambda_0}{\lambda_g}\cos\theta\right)\vec{j} - D\sin\theta\left(1 + \frac{\lambda_0}{\lambda_g}\cos\theta\right)\vec{k}\,. \tag{18}$$

In equation (18), the electric-field component E_z is neglected, since this component is zero in a rectangular waveguide operating in the TE$_{10}$ mode. Then, expression (18) can be written as

$$\vec{E}(E)=D\cos\theta\left(1+\frac{\lambda_0}{\lambda_g}\cos\theta\right)\vec{j}\,. \tag{19}$$

When $\varphi=\pi/2$, expression (9) is significantly simplified and takes the form

$$D=AZ_0\frac{a^2b}{\lambda_0^2}\cdot\frac{1}{\left(-\pi^2/4\right)}\cdot\frac{\sin\left[\left(\pi b/\lambda_0\right)\sin\theta\right]}{\left[\left(\pi b/\lambda_0\right)\sin\theta\right]}\,. \tag{20}$$

After substituting (20) into (19) we obtain

$$\vec{E}(E)=AZ_0\frac{a^2b}{\lambda_0^2}\cdot\frac{1}{\left(-\pi^2/4\right)}\cdot\frac{\sin\left[\left(\pi b/\lambda_0\right)\sin\theta\right]}{\left[\left(\pi b/\lambda_0\right)\sin\theta\right]}\times\left[\cos\theta\left(1+\frac{\lambda_0}{\lambda_g}\cos\theta\right)\right]\vec{j}. \tag{21}$$

Expression (21) determines the RP of a rectangular aperture with the TE_{10} mode in the plane of the $\vec{E}$ vector (Fig. 1, the $y0z$ plane). From (21) it is clear that in this plane the RP is determined by the relation

$$\sin\left[\left(\pi b/\lambda_0\right)\sin\theta\right]/\left[\left(\pi b/\lambda_0\right)\sin\theta\right].$$

This behavior of the radiation pattern in the specified plane occurs when a rectangular aperture is excited by a mode with uniform amplitude and phase. The TE_{10} mode exhibits exactly this field distribution.

In (21) set $\theta=0$. Then, transitioning to scalar quantities and taking into account that at $\theta\to0$ both the ratio $\sin\left[\left(\pi b/\lambda_0\right)\sin\theta\right]/\left[\left(\pi b/\lambda_0\right)\sin\theta\right]$ and $\cos\theta=1$ tend to unity, we write (21) in its final form

$$E^{\max}(E)=AZ_0\frac{a^2b}{\lambda_0^2}\cdot\frac{1}{\left(-\pi^2/4\right)}\cdot\left(1+\frac{\lambda_0}{\lambda_g}\right). \tag{22}$$

Using equations (21) and (22), expression that defines the normalized RP of a rectangular aperture of cross-section $a \times b$, excited by the TE_{10} mode, in the plane of the electric-field vector $\vec{E}$ (Fig. 1, plane $y0z$) can be written:

$$\frac{E(E)}{E^{\max}(E)}=20\lg\left[\frac{1}{\left[1+\left(\lambda_0/\lambda_g\right)\right]}\cdot\frac{\sin\left[\left(\pi b/\lambda_0\right)\sin\theta\right]}{\left[\left(\pi b/\lambda_0\right)\sin\theta\right]}\times\cos\theta\left(1+\frac{\lambda_0}{\lambda_g}\cos\theta\right)\right]. \tag{23}$$

Equations (18) and (24) describe the RP of a rectangular aperture excited by the TE_{10} mode in two mutually perpendicular planes, ($\vec{H}$) and ($\vec{E}$).

We now analyze the RP of a pyramidal horn with transverse aperture dimensions $a_{aperture}\times b_{aperture}$ of 40 × 33 mm^2. The horn transitions into a rectangular waveguide with a cross-section of $a \times b$ = 7.2 × 3.4 mm^2, which supports the propagation of the TE_{10} mode. The external appearance of the horn is shown in Fig. 2. For the RP calculation, we employ equations (17) and (23).

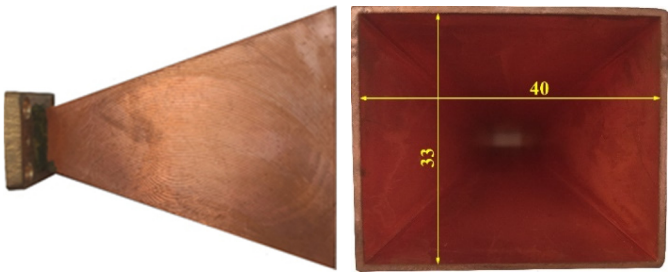

Figure 2. Pyramidal horn

The operating frequency in the K_a-band is chosen within the atmospheric transparency window. To determine this, we use the dependency constructed based on the results reported in [18]. Its behavior is described using an approximate physical model based on the recommendations of ITU-R P.676-12, combined with an absorption continuum model for water vapor and oxygen (Fig. 3).

The figure shows that the minimum atmospheric attenuation occurs in the 30–35 GHz frequency range. The narrow absorption peak at 35.5 GHz corresponds to the water-vapor line, while near 40 GHz the attenuation gradually increases due

to the oxygen absorption continuum. Based on these data, the operating frequency was selected as 34 GHz (λ_0 = 8.824 mm). As seen in Fig. 3, the atmospheric attenuation at this frequency is approximately 0.04 dB/km. Using the expression provided above, the wavelength in the rectangular waveguide, λ_g is equal to 11.166 mm (a = 7.2 mm). To construct the RP (Fig. 2) in two mutually perpendicular planes, it is necessary to determine the distance R from the aperture to the far-field zone. This distance is given by the following expression [19]:

$$R \geq 2a_{aperture}^2 / \lambda_0 . \tag{24}$$

Here, $a_{aperture}$ = 40 mm is the larger aperture dimension. The far-field region is of particular interest when analyzing the RP of any antenna, since the angular distribution of the electric field strength in this region is practically independent of the distance from the antenna. For the radiator under consideration, this region can be determined from inequality (24) and begins at a distance of $R \geq 362.647$ mm. For further analysis, a distance of R = 363 mm was selected. Let us now examine the radiation pattern of the pyramidal horn (Fig. 2).

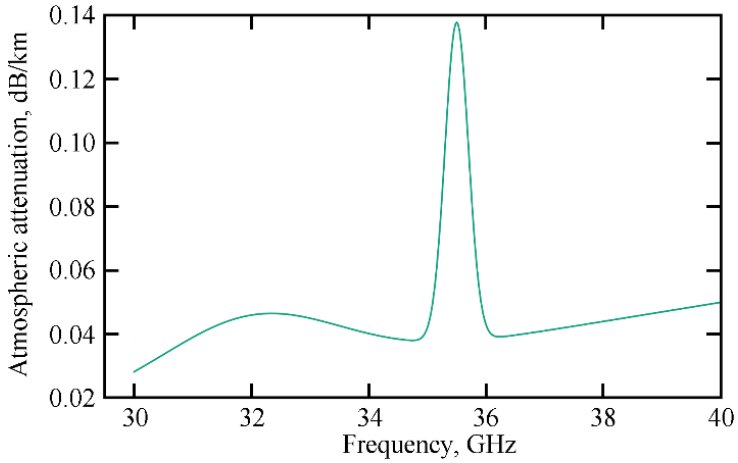

Figure 3. Atmospheric attenuation of electromagnetic radiation in the 30–40 GHz frequency range

In this analysis, we are interested not in the angular dependence itself, but in the cross section of the RP in the $x0z$ plane (the $\vec{H}$ -plane). The meridional angle θ appearing in equation (17) is defined as $\theta = \arctan(x/R)$ (Fig. 1). The calculation results, taking into account this definition, are shown in Fig. 4 ($a_{aperture}$ = 40 mm, red curve). As the next step, the cross section of the pyramidal horn pattern (Fig. 2) was constructed in the $y0z$ plane (the $\vec{E}$ -plane). In this case, the angle $\theta = \arctan(y/R)$ is defined accordingly. The calculation results obtained using equation (24) are presented in Fig. 4 ($b_{aperture}$ = 33 mm, blue curve).

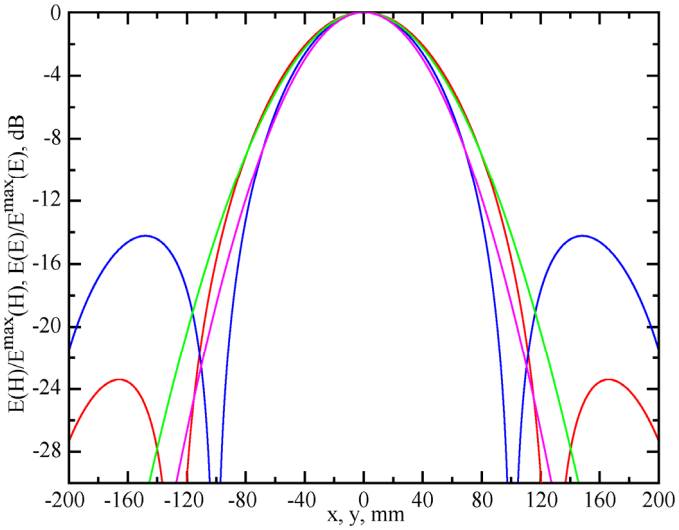

Figure 4. Cross sections of the RP of the pyramidal horn in the image plane

As can be seen, the cross section of the RP of the horn radiator in the image plane of the $\vec{E}$ vector is narrower than that in the $\vec{H}$ -plane. This behavior is explained by the different amplitude variation of the electric field in the aperture of the radiator excited by the TE_{10} mode along the $x0z$ and $y0z$ planes (Fig. 1). Consequently, the RP of the pyramidal horn (Fig. 2)

is not axially symmetric in the far-field region (R = 363 mm). In the $\vec{E}$-plane, an increase in the side-lobe level is observed: −14.23 dB compared to −23.45 dB in the $\vec{H}$-plane (Fig. 4). The Gaussian beam radius is determined at the 1/e level corresponding to −8.686 dB. Let us compare the RP cross section of the pyramidal horn in the $\vec{H}$-plane with a Gaussian field distribution. In this plane, the half-width of the main lobe of the RP, determined at the −8.686 dB level, is taken to correspond to the beam radius w of the Gaussian field distribution. The calculated value of w is 78.351 mm (Fig. 4). The Gaussian field distribution is represented in the form $\exp\left(-x^2/78.351^2\right)$, and the results obtained using equation $E_G(H) = 20\lg\left[\exp\left(-x^2/78.351^2\right)\right]$ are shown in Fig. 4 (green curve). Next, let us compare the RP cross section in the image plane of the $\vec{E}$ vector with the Gaussian field distribution. In this plane, the value of w at the −8.686 dB level is 68.467 mm. The calculation results obtained using equation $E_G(E) = 20\lg\left[\exp\left(-x^2/68.467^2\right)\right]$ are shown in Fig. 4 (pink curve). As can be seen, up to the level of $20\lg\left[E(H)/E^{\max}(H)\right] = -10$ dB, the amplitude distribution of the electric-field component of the pyramidal horn in the far-field region in both the $\vec{H}$- and $\vec{E}$-planes coincides with the Gaussian field distribution. The main drawback of such a pyramidal horn is its axially asymmetric RP. This limitation can be mitigated by reducing the aperture dimension $b_{aperture}$.

The paper [20] shows that the condition for negligible diffraction losses in an open resonator supporting oscillations with a Gaussian field distribution is determined by the relation $G = 4w$, where G is the resonator mirror diameter. Therefore, the condition for negligible diffraction losses during the incidence of a Gaussian beam on an optical element with the specified dimensions in the $\vec{H}$-plane is satisfied if the beam diameter is at least 313.4 mm. This plane is considered because its RP cross section in the image plane is larger. As can be seen, this is a rather large diameter for the K_a-band. To reduce it, the size of the wide side of the pyramidal horn $a_{aperture}$ must be increased. However, doing so leads to an increase in the parameter R according to inequality (24) and, consequently, to an increase in the Gaussian beam radius. Therefore, a reasonable compromise between these parameters is required.

Fig. 5 shows cross sections of the RP of the pyramidal horn in the image plane of the $\vec{H}$ vector for the TE_{10} mode of a rectangular aperture at three values of the wide-side dimension: $a_{aperture}$ = 40 mm (R = 363 mm, red curve), $a_{aperture}$ = 50 mm (R = 567 mm, blue curve), and $a_{aperture}$ = 60 mm (R = 816 mm, green curve).

It can be seen from the figure that the Gaussian spot diameter increases as the value of $a_{aperture}$ increases. It is also evident that enlarging the dimension $a_{aperture}$ makes it impossible to achieve an axially symmetric field distribution.

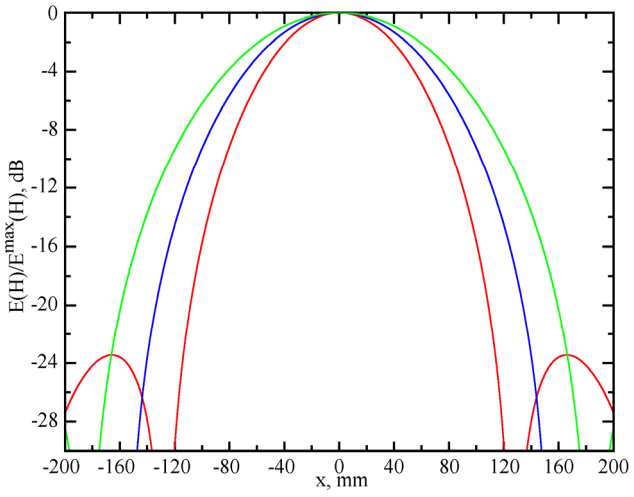

Figure 5. Cross sections of the RP of the pyramidal horn in the image $x0z$ plane for increasing values of the wide side $a_{aperture}$

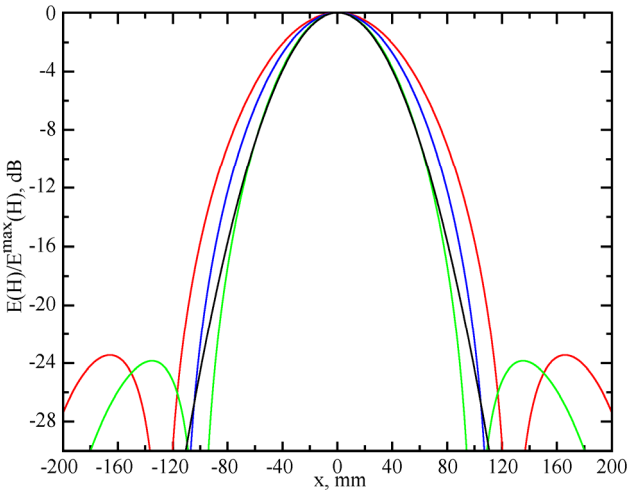

Figure 6. Cross sections of the RP of the pyramidal horn in the image $x0z$ plane for decreasing values of the wide side $a_{aperture}$

Let us now consider the case when the larger side of the rectangular aperture $a_{aperture}$ is reduced. The calculation results in the plane of the $\vec{H}$ vector, obtained using expression (18), are presented in Fig. 6. The cross-sections of the RP in the image plane are shown for the following cases: $a_{aperture}$ = 40 mm (R = 363 mm, red curve); $a_{aperture}$ = 35 mm (R = 278 mm, blue curve); and $a_{aperture}$ = 30 mm (R = 204 mm, green curve). It is clearly seen that as $a_{aperture}$ decreases, the RP becomes narrower in the far-field region. This occurs due to the corresponding decrease of the parameter R (see (24)). Let us now compare the

field distribution in the $\vec{H}$ -plane for $a_{aperture}$ = 30 mm with the Gaussian distribution. As before, the field spot radius w is determined at the –8.686 dB level and is equal to 59.527 mm (Fig. 6). The distribution of the electric field component according to the Gaussian law $E_G(H) = 20\lg\left[\exp\left(-x^2/59.527^2\right)\right]$, is shown in Fig. 6 (black curve). It follows from the figure that the cross-section of the RP in the image $\vec{H}$ -plane when $E_G(H) = 20\lg\left[\exp\left(-x^2/59.527^2\right)\right]$ = 30 mm coincides with the Gaussian field distribution down to approximately the –10 dB level. This result confirms the earlier conclusion that the RP of a rectangular aperture in the $\vec{H}$ - and $\vec{E}$ -planes exhibits an electric field distribution that agrees with the Gaussian one up to the –10 dB level.

Let us determine the required diameter of the optical element placed at a distance of R = 204 mm from the aperture (in the Fraunhofer zone). The condition for negligible diffraction losses of a Gaussian beam incident on the optical element will be satisfied if the beam diameter equals $4w$=238.084 mm [20]. Therefore, the optical element diameter is chosen to be 240 mm. It follows that, in this case, the optical element also has considerable geometric dimensions in the K_a-band, approximately $27\lambda_0$.

To obtain an axially symmetric distribution of the electric field component in the far-field region at a distance of 204 mm from the aperture ($a_{aperture}$ =30 mm), it is necessary to reduce the size of its narrow side $b_{aperture}$. The results of the calculations in the plane of the E-vector, performed in accordance with (23), are presented in Fig. 7. The red curve corresponds to the RP cross-section in the H-plane ($a_{aperture}$ =30 mm). As can be seen from Fig. 7, side lobes appear in the RP cross-section, with an amplitude of –23.85 dB. When the narrow side of the pyramidal horn is reduced to $b_{aperture}$ =21.539 mm, the RP cross-section in the E-plane (blue curve) at a distance of 204 mm from the aperture increases to the –12 dB level and practically coincides with the RP cross-section in the H-plane. This correspondence holds for the main lobe of the RP. The side-lobe level for this value of $b_{aperture}$ decreases to –15.73 dB, compared to –14.23 dB for $b_{aperture}$ =33 mm (see Fig. 4).

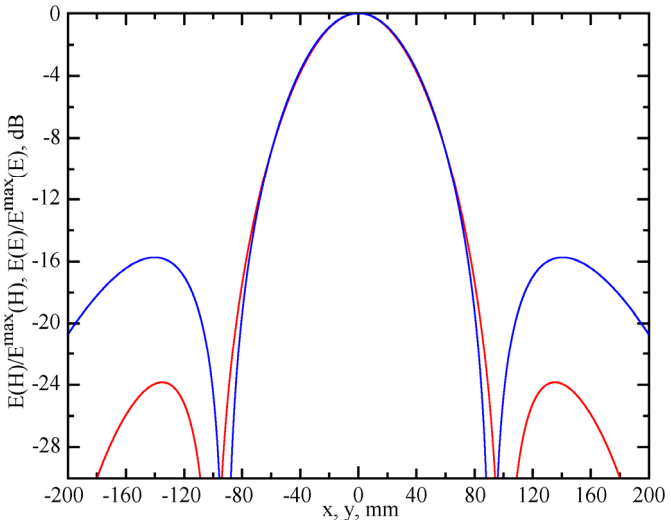

Figure 7. Cross sections of the RP of the pyramidal horn in the $x0z$ and $y0z$ planes when the aperture dimension was decreased down to $b_{aperture}$ = 21.539 mm

The calculations were performed under the assumption that the TE_{10} mode exists in both the aperture and the waveguide. The electric field distribution of this mode in the aperture, in the $x0z$ plane (Fig. 1), must be in phase. The length of the horn radiator should therefore be chosen to ensure the required phase distribution across the aperture.

The maximum phase error in the aperture is determined by the geometric dimensions of the horn. Its permissible value must satisfy the following condition [19]:

$$\zeta_{\max} = \frac{\pi a_{aperture}^2}{4\lambda_0 R_H} \le \frac{3}{4}\pi, \qquad (\vec{H}\text{-plane}) \tag{25}$$

$$\xi_{\max} = \frac{\pi b_{aperture}^2}{4\lambda_0 R_E} \le \frac{\pi}{2}. \qquad (\vec{E}\text{-plane}) \tag{26}$$

Here: R_H and R_E are the distances from the aperture to the point where the edges of the horn converge in the planes of the $\vec{H}$ and $\vec{E}$ vectors of TE_{10} mode in the waveguide.

On the other hand, the quantities R_H and R_E are related to the aperture dimensions $a_{aperture}$, $b_{aperture}$ and to the waveguide dimensions a, b by the relation [19]:

$$\frac{R_H}{R_E}=\frac{a_{aperture}}{b_{aperture}}\cdot\frac{\left(b_{aperture}-b\right)}{\left(a_{aperture}-a\right)}. \tag{27}$$

From inequality (24) it follows that $R_H\geq 34$ mm that allows us to select R_H=40 mm. The cross sections of the rectangular waveguide and of the radiating aperture are $a\times b$ = 7.2 × 3.4 mm^2 and $a_{aperture}\times b_{aperture}$=30×21.539 mm respectively. Then, from (27), it follows that R_E=36 mm that satisfies inequality (26).

Let us estimate the reflection coefficient from the designed radiator. This is necessary to determine what fraction of the generator power is actually radiated into free space. In general, reflection in such a radiator occurs at two regions: at the aperture itself ($\dot{\Gamma}_{aperture}$) and at its neck ($\dot{\Gamma}_{neck}$). The reflection coefficient at the aperture, $\dot{\Gamma}_{aperture}$, is a complex quantity whose magnitude and phase depend on the aperture dimensions. As shown in [17, 19], with increasing aperture size, the magnitude of the reflection coefficient decreases, and the phase difference between the aperture center and the edge decreases. For apertures with dimensions of several wavelengths, $\dot{\Gamma}_{aperture}$ can be considered approximately zero. This condition is satisfied for the rectangular aperture under consideration, where $a_{aperture}$=30 mm (≈3.4 λ_0) and $b_{aperture}$=21.539 mm (≈2.45 λ_0).

To determine the magnitude of the reflection coefficient of the designed radiator, the following relation is used:

$$\left|\dot{\Gamma}_{aperture}\right|=\left[1-(\gamma/k)\right]/\left[1+(\gamma/k)\right], \tag{28}$$

where $\gamma=2\pi\sqrt{1-\left(\lambda_0/2a_{aperture}\right)^2}\Big/\lambda_0$ is the propagation constant in a rectangular waveguide whose cross-section is equal to the aperture of the horn ($a_{aperture}$=30 mm), $k=2\pi/\lambda_0$.

The calculation using (28) at a frequency of 34 GHz (λ_0=8.824 mm) resulted in $\left|\dot{\Gamma}_{aperture}\right|$=0.006. Therefore, reflection from a rectangular aperture can be neglected.

Let us now estimate the fraction of the generator power reflected from the neck (phase focus) of the radiator under consideration. The absolute value of the reflection coefficient at the neck $\left|\dot{\Gamma}_{neck}\right|$ can be determined from the following expression [19]:

$$\left|\dot{\Gamma}_{neck}\right|=\left(Z_{equiv}-1\right)/\left(Z_{equiv}+1\right), \tag{29}$$

where

$$Z_{equiv}=1+\frac{1}{a\left(2\pi/\lambda_w\right)\mathrm{ctg}\alpha_0\left(1-\left(\lambda_0/2a\right)^2\right)}-\frac{1}{b\left(2\pi/\lambda_w\right)\mathrm{ctg}\beta_0},$$

$2\alpha_0$ and $2\beta_0$ are the radiator aperture angles in the $\vec{H}$ and $\vec{E}$ planes, respectively; $\alpha_0=\arctan\left(\left(a_{aperture}/2\right)/R_H\right)$, $\beta_0=\arctan\left(\left(b_{aperture}/2\right)/R_E\right)$. For the given dimensions $Z_{equiv}=0.991$ and $\left|\dot{\Gamma}_{neck}\right|=0.005$ and therefore, reflections from both the aperture and the neck can be neglected. This indicates that almost all of the source power is radiated into free space, i.e., a traveling-wave regime is established in the waveguide section.

3. EXPERIMENTAL STUDY

To verify the above calculations, an experimental study was conducted using two pyramidal horns, one of which is shown in Fig. 2. The dimensions of the second radiator which appearance is shown in Fig. 8 were chosen based on the theoretical analysis of the rectangular aperture.

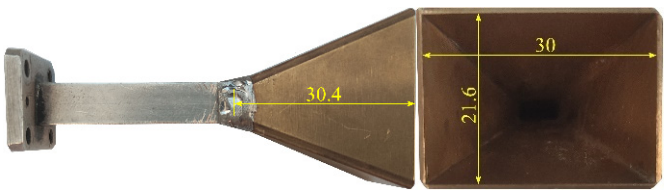

Figure 8. Pyramidal horn with a rectangular waveguide section

Let us consider a horn with rectangular aperture dimensions $a_{aperture} \times b_{aperture}$ =40×33 mm. Using a panoramic VSWR meter R2-65, the VSWR in the waveguide section loaded with this pyramidal horn was measured in the 33–35 GHz frequency range. The measurement results are presented in Fig. 9.

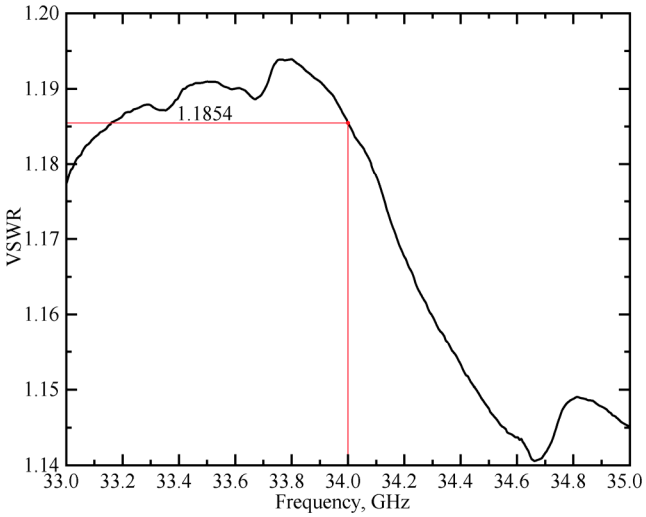

Figure 9. Dependence of the VSWR on frequency in the waveguide section loaded with a rectangular horn having aperture dimensions of 40×33 mm

As can be seen from the figure, at a frequency of 34 GHz the VSWR is 1.1854, which corresponds to a field reflection coefficient from the given aperture of $\Gamma = 0.0848$. The obtained result is in good agreement with the results of [17, 19], where it was shown that the reflection from a rectangular aperture can be neglected if its dimensions exceed several wavelengths.

To measure the RP cross-section of the pyramidal horn in the image plane, an experimental setup was assembled, the block diagram of which is shown in Fig. 10.

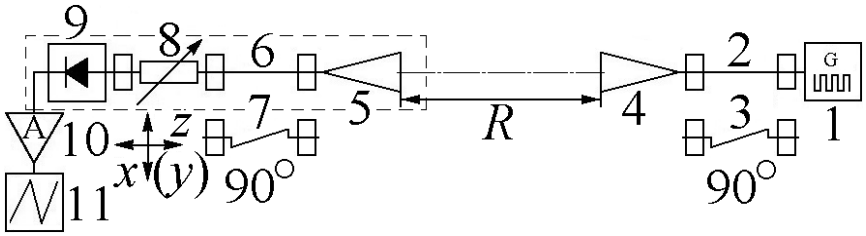

Figure 10. The experimental setup block diagram

As the source 1 of 34 GHz radiation, a high-frequency signal generator G4-156 was used. The main parameters of this generator are as follows: frequency range 29.95–37.5 GHz; output power not less than 5 mW; frequency setting error ±1%. To expand the dynamic range, the output signal was modulated by a rectangular waveform (square wave) with a frequency of 1 kHz.

Between the generator and the investigated horn 4, a 60 mm long section of rectangular waveguide 2 was inserted. In this configuration, the setup makes it possible to measure the RP cross-section of the pyramidal horn in the image plane of the $\vec{H}$ vector of the TE_{10} mode in the waveguide, i.e., in the $x0z$ plane. The receiving path includes: a receiving horn 5, a section of rectangular waveguide 6 identical to the section 2, a polarization attenuator 8, and a detector section 9. The signal from the detector is fed to a resonant amplifier 10 tuned to a frequency of 1 kHz. An oscilloscope 11 is used for visual monitoring of the signal level. Both pyramidal horns 4 and 5 have identical apertures of 40×33 mm. For the investigated horn, the distance R determining the far-field region is 363 mm. The part of the measuring setup enclosed by the dashed line in Fig. 10 allows the receiving horn to be moved along the z-axis over a range of ±25 mm and along the x-axis over a range of ±80 mm.

The results of measuring the RP cross-section of horn 4 in the image plane of the $\vec{H}$ vector are presented in Fig. 11. The experimental values are shown by green circles. The figure also presents the theoretically calculated RP cross-section in the same plane for a horn of the specified dimensions, obtained using formula (17) (red curve).

As can be seen from the figure, there is good agreement between the calculated and measured cross-sections of the RP.

To measure the RP cross-section of horn 4 in the image plane of the $\vec{E}$ vector (the $y0z$ plane), it is necessary to replace the waveguide sections 2 and 6 with 90° waveguide twists 3 and 7 of the same length (Fig. 10). The measurement results are shown in Fig. 12. As in the previous case, good agreement is observed between the measured (green circles) and the calculated, according to formula (23), (blue curve) RP cross-sections in the image plane of the $\vec{E}$ vector.

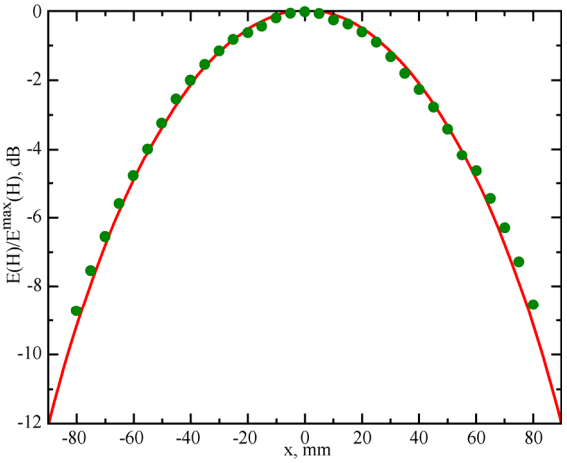

Figure 11. The measured RP cross-section of the pyramidal horn having aperture dimensions of 40×33 mm in the image plane *x*0*z*

From the presented figures, it follows that the RP cross-section of the considered pyramidal horn in the *x*0*z* image plane at the –8.7 dB level (corresponding to the Gaussian field distribution) is wider than in the *y*0*z* image plane. In this case, these cross-sections are 160 mm and 140 mm, respectively. Thus, the experimental results confirm the theoretical conclusion that the pyramidal horn with an aperture of 40×33 mm^2 has an axially asymmetric radiation pattern. In the previous section, a pyramidal horn was designed to provide an axially symmetric RP in the far-field region (Fig. 8).

Using a panoramic VSWR meter R2-65, the VSWR was measured in a waveguide line loaded with a pyramidal horn having an aperture of 30×21.6 mm^2 in the same frequency band. The measurement results are shown in Fig. 13.

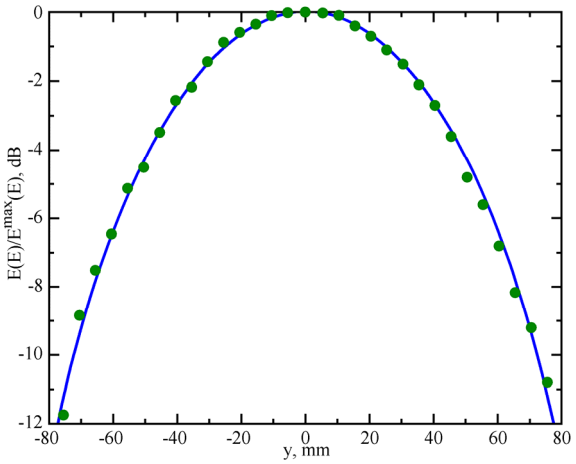

Figure 12. The measured RP cross-section of the pyramidal horn having aperture dimensions of 40×33 mm^2 in the image plane *y*0*z*

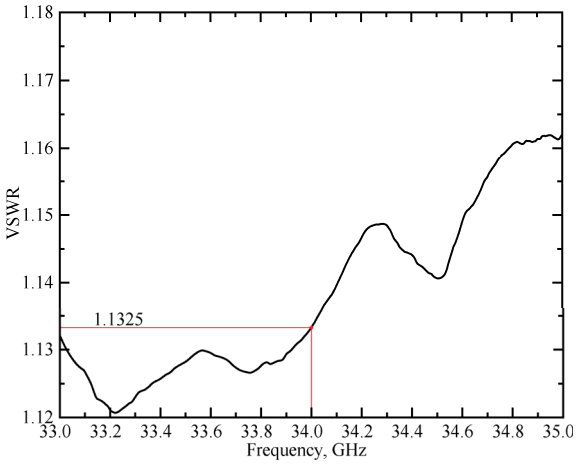

Figure 13. The measured VSWR dependence on frequency in the waveguide line loaded with a rectangular horn having an aperture size of 30×21.6 mm^2

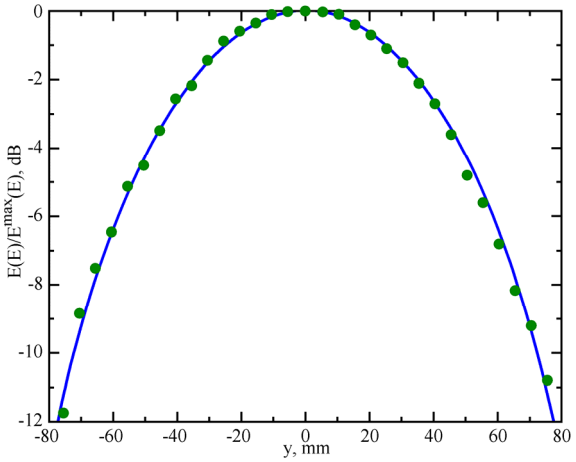

Figure 12. The measured RP cross-section of the pyramidal horn having aperture dimensions of 40×33 mm^2 in the image plane *y*0*z*

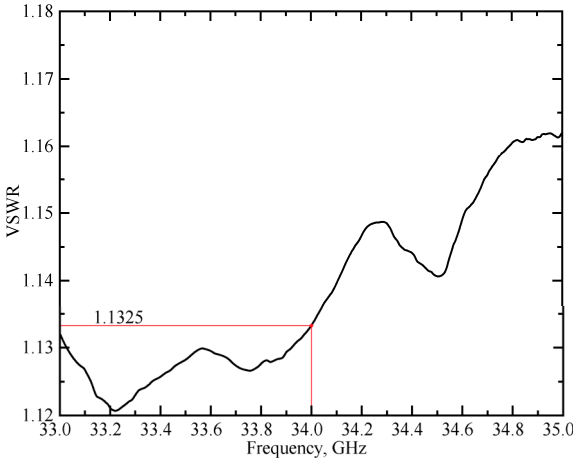

Figure 13. The measured VSWR dependence on frequency in the waveguide line loaded with a rectangular horn having an aperture size of 30×21.6 mm^2

As can be seen from the figure, in this case, at a frequency of 34 GHz, the VSWR = 1.1325, which corresponds to a field reflection coefficient of $\Gamma = 0.0621$. The obtained result correlates well with the calculated data for this horn presented in the previous section. Thus, the reflection from the aperture of such a radiator can be neglected.

Now let us consider the RP cross-section of this horn in the image plane. To carry out the measurements on the experimental setup, horn 4 was replaced with the test radiator having the specified aperture dimensions. For this horn, the distance R=204 mm. Instead of the receiving horn 5, an open end of a rectangular waveguide with a cross-section of 7.2×3.4 mm^2 was placed at the specified distance. The results of the radiation pattern cross-section measurements in the image plane of the $\vec{H}$ -vector of the TE$_{10}$ mode in waveguide 2 are shown in Fig. 14.

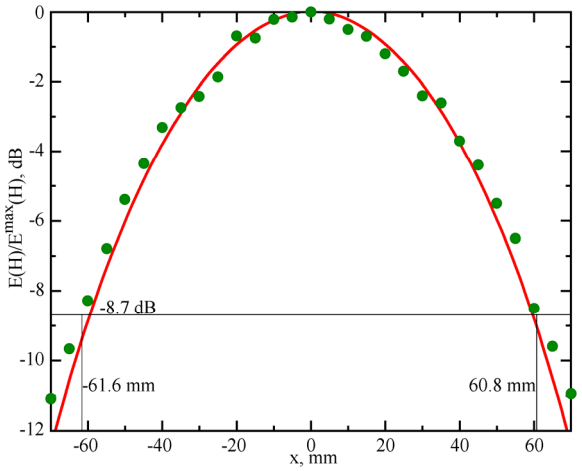

Figure 14. The measured RP cross-section of the pyramidal horn having aperture dimensions of 30×21.6 mm^2 in the image plane $x0z$

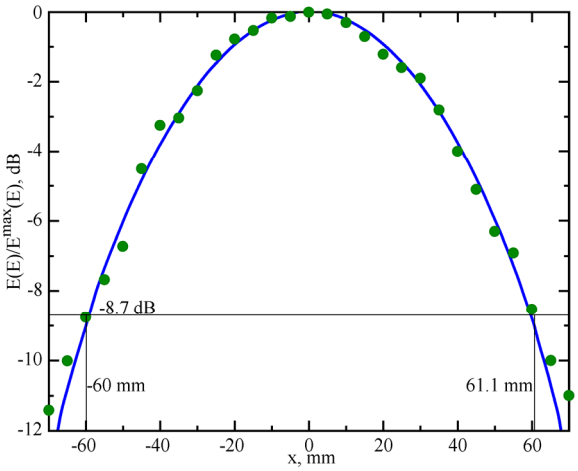

Figure 15. The measured RP cross-section of the pyramidal horn having aperture dimensions of 30×21.6 mm^2 in the image plane $y0z$

From the figure, a good agreement can be seen between the measured RP cross-section in the specified image plane (green circles) and the one calculated using formula (18) (red curve). At the –8.7 dB level (corresponding to the Gaussian field distribution), the radiation pattern cross-section width is 122.4 mm. For comparison, let us consider the RP cross-section of the rectangular aperture in the picture plane of the $\vec{E}$ vector. As in the previous case, the waveguide sections 2 and 6 are replaced with 90° waveguide twists 3 and 7 of the same length (see Fig. 10). The measurement results are shown in Fig. 15. In this case, there is also good agreement between the experimentally measured and the calculated radiation pattern cross-sections in the image plane $y0z$. The RP cross-section width at the –8.7 dB level is 121.1 mm. Thus, the designed pyramidal horn produces an axially symmetric radiation pattern in the far-field region. However, using such a pyramidal horn for the intended purpose is impractical due to the large field spot size at the –8.7 dB level in the far-field region. In this case, to ensure negligible diffraction losses when a Gaussian beam is incident on the flat face of the axicon, its diameter must be approximately1 240 mm. This represents unreasonably large geometric dimensions of the optical element in the K_a-band.

4. CONCLUSIONS

The studies of the rectangular aperture performed in the first part of the paper make it possible to draw several important practical conclusions.

1. By varying the aperture dimensions $a_{aperture} \times b_{aperture}$, it is always possible to obtain an axially symmetric radiation pattern of such a radiator in the far-field region. This is due to the linear distribution of the electric field in the aperture.
2. Up to the –8.7 dB level, the radiation pattern cross-sections of such a radiator in two mutually perpendicular planes coincide with the Gaussian field distribution.
3. Depending on the specific application, it is always necessary to find a compromise between the aperture dimensions $a_{aperture} \times b_{aperture}$ and the distance R to the far-field region.
4. For the chosen geometric dimensions of rectangular apertures in the K_a-band, a traveling-wave regime is established in the waveguide section.
5. In the K_a-band, the optical element must have large geometric dimensions (~$27\lambda_0$) in order to minimize diffraction losses when a Gaussian beam is incident on its flat surface. Therefore, when using a rectangular aperture with an axially symmetric radiation pattern in the far-field region and an acceptable distance $R = (20 \div 23)\lambda_0$, the geometric dimensions of the axicon become unreasonably large.
6. It is of practical interest to consider radiating apertures of other shapes that would allow obtaining narrower radiation pattern cross-sections in the far-field region.

Acknowledgement

This work was supported by the National Research Foundation of Ukraine (Project No. 2025.06/0011).

ORCID
I.K. Kuzmychov, https://orcid.org/0000-0002-6870-5491; **O.A. Voitovych,** https://orcid.org/0000-0001-7530-5149;
O.S. Lukash, https://orcid.org/0009-0008-2408-3644; **E.M. Khutoryan,** https://orcid.org/0000-0002-0727-7753;
V.P. Maltsev, https://orcid.org/0009-0002-7523-7603

REFERENCES

[1] Y. Dewen, T. Yan, C. Changhua, Z. Feng, and H. Lei, High Power Laser and Particle Beams, **37** (2025). https://doi.org/10.11884/HPLPB202537.240374
[2] S. Mumtaz, H.S. Uhm, and E.H. Choi, Physics Reports, **1069**, 1 (2024). https://doi.org/10.1016/j.physrep.2024.03.003
[3] C.-H. Zhan, T.-M. Li, L. Meng, Z.-H. Li, Y. Wu, and J.-B. Shao, Acta Phys. Sin. **63**, 238405 (2014). https://doi.org/10.7498/aps.63.238405
[4] Y. Xu, Review of the high-power vacuum tube microwave sources, arXiv:2003.04288 [physics.plasm-ph] (2024).
[5] E. Negri, W. Fuscaldo, P. Burghignoli, and A. Galli, Micromachines, **13**, 2230 (2022). https://doi.org/10.3390/mi13122230
[6] Z. Yu, and W.B. Dou, Prog. Electromagn. Res. **93**, 205 (2009). https://doi.org/10.2528/PIER09032303
[7] H. Huang, and Y. Yu, Acta Tech. **62**, 107 (2017).
[8] S. Monk, J. Arlt, D.A. Robertson, J. Courtial, and M.J. Padgett, Opt. Commun. **170**, 213 (1999). https://doi.org/10.1016/S0030-4018(99)00297-7
[9] H. Meng, B. Xiang, J. Zhang, W. Dou, and Y. Yu, J. Infrared Millim. Terahertz Waves, **35**, 208 (2014). https://doi.org/10.1007/s10762-013-0044-3
[10] V. Jarutis, R. Paskauskas, and A. Stabinis, Opt. Commun. **184**, 105 (2000). https://doi.org/10.1016/S0030-4018(00)00945-4
[11] S. Cabrini, C. Liberale, D. Cojoc, A. Carpentiero, M. Prasciolu, S. Mora, V. Degiorgio, *et al*., Microelectr. Engineer. **83**(4-9), 804-807 (2006). https://doi.org/10.1016/j.mee.2006.01.247
[12] M. Ettorre, S. Pavone, M. Casaletti, M. Albani, A. Mazzinghi and A.Freni, *Aperture Antennas for Millimeter and Sub-Millimeter Wave Applications*, (Springer, Cham, 2017). https://doi.org/10.1007/978-3-319-62773-1_8
[13] Z. Zhai, Z. Cheng, Q. Lv, and X. Wang, Appl. Sciences, 10(15), 1-11 (2020). https://doi.org/10.3390/app10155127
[14] J. Dudutis, M. Mackevičiūtė, J. Pipiras, R. Stonys, V. Stankevič, G. Račiukaitis, and P. Gečys, Opt. Express, **30**(2), 1860-1874 (2022). https://doi.org/10.1364/OE.447035
[15] C. Lyu, M. R. Belić, Y. Li, and Y. Zhang, Optics & Laser Technology, **164**, 109548 (2023). https://doi.org/10.1016/j.optlastec.2023.109548
[16] M. Eskandari, M. Joodaki, and A.R. Attari, arXiv:2408.03333 [physics.app-ph], 1-11 (2024). http://dx.doi.org/10.1109/TMTT.2024.3449650
[17] R. Kühn, *Mikrowellenantennen*, (VEB Verlag Technik, Berlin, 1964).
[18] J.R. Pardo, J. Cernicharo, and E. Serabyn, IEEE Trans. Antennas Propag., **49**(12), 1683-1694 (2001). http://dx.doi.org/10.1109/8.982447
[19] C.A. Balanis, *Antenna Theory: Analysis and Design*, 3rd ed. (Wiley, Hoboken, NJ, 2005). https://doi.org/10.1002/0471654507
[20] D. Gloge, *Proceedings of the symposium on quasi-optics*, (Polytechnic Press, Brooklyn, 1964).

ОТРИМАННЯ АКСІАЛЬНО-СИМЕТРИЧНОГО РОЗПОДІЛУ ПОЛЯ З ВИКОРИСТАННЯМ ПРЯМОКУТНИХ АПЕРТУРНИХ ВИПРОМІНЮВАЧІВ

І.К. Кузьмичов[1], О.А. Войтович[1], О.С. Лукаш[1], Е.М. Хуторян[1], В.П. Мальцев[1], О.В. Май[2]
[1]Інститут радіофізики та електроніки ім. О. Я. Усикова НАН України,вул. Ак. Проскури 12., Харків, 61085, Україна
[2]ТОВ "Актокс Україна", вул. І. Гонти, 1, Київ, 04112, Україна

У роботі з використанням апертурного методу досліджено випромінювання з відкритого кінця прямокутного хвилеводу. Отримано вирази, що описують діаграму спрямованості (ДС) такої апертури в дальній зоні у двох взаємно перпендикулярних площинах. Для конкретних розмірів двох прямокутних апертур 40×33 мм та 30×21,6 мм проведено чисельні дослідження перерізів ДС у картинній площині за змінних ширини та довжини сторін розкривів. Зроблено порівняння отриманих перерізів ДС з Гаусовим розподілом поля та встановлено, що до рівня -11 дБ, перерізи ДС в обох картинних площинах практично збігаються з Гаусовим розподілом поля. Це особливо важливо під час падіння хвильового пучка на плоску грань аксікону. При зміні розміру вузької сторони прямокутної апертури можна отримати аксіально-симетричну ДС. Проведено експериментальні дослідження цих прямокутних апертур у K_a діапазоні. Показано гарний збіг експериментальних результатів із розрахунковими даними. Встановлено, що якщо геометричні розміри прямокутної апертури перевищують дві довжини хвилі, то в хвилеводному тракті встановлюється режим біжучої хвилі. Експериментально виявлено, що амплітудний розподіл поля обох апертур у дальній зоні до рівня −8,7 дБ збігається з Гауссовим розподілом поля. Показано, що для опромінення плоскої грані аксікону хвильовим пучком використовувати прямокутні апертури не доцільно.

Ключові слова: *апертурний метод; K_a діапазон; прямокутна апертура; діаграма спрямованості; Гауссовий розподіл поля; аксікон*